IOPscience iopscience.iop.org

Home Search Collections Journals About Contact us My IOPscience

Humidity sensing using vertically oriented arrays of ReS_2 nanosheets deposited on an interdigitated gold electrode

This content has been downloaded from IOPscience. Please scroll down to see the full text.

2016 2D Mater. 3 045012

(http://iopscience.iop.org/2053-1583/3/4/045012)

View the table of contents for this issue, or go to the journal homepage for more

Download details:

IP Address: 129.161.157.204
This content was downloaded on 26/10/2016 at 14:09

Please note that terms and conditions apply.

You may also be interested in:

Synthesis, properties and applications of 2D non-graphene materials
Feng Wang, Zhenxing Wang, Qisheng Wang et al.

Liquid exfoliated pristine WS2 nanosheets for ultrasensitive and highly stable chemiresistive humidity sensors
Ravindra Kumar Jha and Prasanta Kumar Guha

Stable electrical performance observed in large-scale monolayer WSe2(1x)S2x with tunable band gap
Jian Huang, Wenhui Wang, Qi Fu et al.

High-performance flexible hydrogen sensor made of WS2 nanosheet-Pd nanoparticle composite film
Cihan Kuru, Duyoung Choi, Alireza Kargar et al.

The role of defects and doping in 2D graphene sheets and 1D nanoribbons
Humberto Terrones, Ruitao Lv, Mauricio Terrones et al.

A novel humidity sensor based on alumina nanowire films
Zhe-sheng Feng, Xin-Jie Chen, Jin-ju Chen et al.

Universal low-temperature Ohmic contacts for quantum transport in transition metal dichalcogenides
Shuigang Xu, Zefei Wu, Huanhuan Lu et al.

2D Materials

PAPER

Humidity sensing using vertically oriented arrays of ReS_2 nanosheets deposited on an interdigitated gold electrode

RECEIVED
2 August 2016

ACCEPTED FOR PUBLICATION
30 September 2016

PUBLISHED
17 October 2016

Aijun Yang[1,2,7], **Jian Gao**[1,7], **Baichang Li**[1], **Jiawei Tan**[1], **Yu Xiang**[3], **Tushar Gupta**[4], **Lu Li**[4], **Shravan Suresh**[4], **Juan Carlos Idrobo**[5], **Toh-Ming Lu**[3,6], **Mingzhe Rong**[2] **and Nikhil Koratkar**[1,4]

[1] Department of Materials Science and Engineering, Rensselaer Polytechnic Institute, Troy, NY 12180, USA
[2] State Key Laboratory of Electrical Insulation and Power Equipment, Xi'an Jiaotong University, 710049, People's Republic of China
[3] Department of Physics, Applied Physics, and Astronomy, Rensselaer Polytechnic Institute, Troy, NY 12180, USA
[4] Department of Mechanical Engineering, Rensselaer Polytechnic Institute, Troy, NY 12180, USA
[5] Center for Nanophase Materials Sciences, Oak Ridge National Laboratory, Oak Ridge, TN 37831, USA
[6] Center for Materials, Device, and Integrated Systems, Rensselaer Polytechnic Institute, Troy, NY 12180, USA
[7] These authors contributed equally to this work.

E-mail: koratn@rpi.edu

Keywords: humidity sensing, sensitivity, hysteresis, ReS_2 nanosheets, chemical vapor deposition

Abstract

We report a novel humidity sensor featuring vertically oriented arrays of ReS_2 nanosheets grown on an interdigitated gold electrode by chemical vapor deposition. The vertical orientation of the nanosheets is important since it maximizes the exposed surface area for water adsorption/desorption. We find that the resistance of the ReS_2 film decreases sensitively with increasing relative humidity, which we attribute to charge transfer from the absorbed H_2O molecules to the n-doped ReS_2 nanosheets. In addition to high sensitivity, the ReS_2 sensors exhibit fast response/recovery time and excellent reversibility with minimal hysteresis. Moreover, our fabrication approach involving the direct (1-step) growth of the ReS_2 films on an interdigitated electrode (without any transfer using wet chemistry or lithography) greatly simplifies the device architecture and has important practical benefits for the low-cost and scalable deployment of such sensor devices.

Introduction

Recent years have witnessed increasing interest in 2D nanomaterials, such as graphene and transition metal dichalcogenides (TMDs), due to their unique blend of physical, chemical, electronic and optical properties [1, 2]. In particular, 2D materials hold great potential for gas sensing due to their inherently high surface-to-volume ratio. For example, physisorbed small molecules were found to modify carrier density and thus change the conductivity of 2D nanomaterials [3, 4]. While initial efforts were focused on graphene, such graphene based sensors can be problematic in terms of reversibility and selectivity [5, 6]. Of late, TMDs have attracted interest for chemical sensing and revealed better performance in some cases [7]. Very recently, a new member of the TMD family, ReS_2, has attracted significant research interest due to its in-plane anisotropic structure. Unlike the common hexagonal layered dichalcogenides such as MoS_2, WS_2, $MoSe_2$, and WSe_2, ReS_2 forms a stable distorted 1 T structure with triclinic symmetry due to an additional valence electron in rhenium [8]. It has been recently reported that the photo-response of ReS_2 transistors could be modulated by adsorbed gas species [9], which suggests that ReS_2 could in-fact serve as a promising 2D material for chemical sensing applications.

In this work, we explore the use of ReS_2 nanosheets for humidity sensing. Detection of humidity is important in various industrial processes and environments [10], such as manufacturing processes control and intelligent control of living environments. Recent efforts have significantly improved the performance of humidity sensors based on 2D materials in terms of their response/recovery times [11–14]. However, for commercial viability of such 2D materials based sensors, it is important to simplify the sensor fabrication process while also minimizing sensor hysteresis. Here, we report the fabrication of a new device architecture featuring vertically oriented arrays of ReS_2 nanosheets grown on an interdigitated gold electrode by chemical vapor deposition (CVD) in a single (1-step) process.

© 2016 IOP Publishing Ltd

The as-grown ReS_2 films were systematically characterized by scanning electron microscopy (SEM), x-ray diffraction (XRD) and scanning transmission electron microscopy (STEM). Individual ReS_2 sheets were also extracted from the CVD grown films and used as the active element in a field effect transistor (FET) device. The FET tests revealed that the ReS_2 nanosheets exhibit n-type semiconductor characteristics. Therefore when exposed to water, electron injection into the sheets from adsorbed water molecules increases the doping in the material causing a large increase in its electrical conductivity. This increase in the conductivity for the CVD grown ReS_2 films could be detected using simple electrical readout (from the interdigitated electrode device) and correlated to the relative humidity. The ReS_2 sensor reported here showed high sensitivity for humidity detection along with fast response/recovery time and significantly low hysteresis. This can be attributed to the vertical orientation of the ReS_2 sheets, which exposes the full surface area of the 2D material for the rapid adsorption/desorption of water.

We would like to point out that direct growth of the ReS_2 films on an interdigitated electrode (without any transfer) as in our device has important implications for low cost and mass producible devices. So far, most electronic sensors made using TMDs are based on manual mechanical exfoliation of monolayer to few-layer flakes. Such methods involving manual exfoliation are averse to mass production and reproducibility. CVD methods have also been used to grow TMDs on SiO_2/Si or sapphire substrates, but these methods damage the substrate and require transfer of the TMD sheet using chemical wet processing methods. Further, e-beam lithography to electrically address the flakes is complicated and expensive, thus hindering their practical applications. In our device, we overcome the above limitations by direct (1-step) growth of vertically oriented ReS_2 nanosheets onto an interdigitated electrode pattern that is used for electrical readout of the sensor device.

Results and discussions

Keyshar *et al* [15], He *et al* [16] and Zhang *et al* [17] have reported the growth of ReS_2 by CVD. In these works, the ReS_2 sheets grew parallel to the growth substrate. By contrast, we have grown vertical ReS_2 by selecting ReO_3 as the precursor for CVD growth and by appropriate tuning of the growth conditions. Figure 1(a) illustrates the scheme for the growth of ReS_2 by CVD method. Briefly, ~1 mg rhenium trioxide (ReO_3) powder is placed in an alumina boat with the substrate facing down and the boat is loaded in the center of the furnace. Sulphur powder is placed upstream within the low-temperature zone and heated by a heating belt. During the ReS_2 growth process, the temperatures are controlled according to the profiles in figure 1(b). Detailed procedure for the growth of ReS_2 can be found in the experimental section. In this work, we have chosen an interdigitated gold electrode pre-patterned on an insulating ceramic wafer as the growth substrate. The schematic of the interdigitated gold electrode is shown in the inset of figure 1(c) with the finger gap of ~10 μm. To fill up the gap, we have tuned the growth conditions to grow high spatial density, vertically-oriented ReS_2. Figures 1(c)–(e) are the SEM images of CVD-grown ReS_2 on the interdigitated electrodes. The ReS_2 sheets tend to grow vertically on both Au and ceramic substrates with high packing density, as indicated by the high-magnification SEM image in figure 1(e). Due to high spatial density of ReS_2 sheets, we expected that the adjacent fingers of the interdigitated electrode are electrically connected by the network of ReS_2 nanosheets. The reason for the vertical growth mode that we observe is not clear at this point but could be related to the rapid supply of Re (from fast evaporation of ReO_3 at our CVD growth conditions) that could suppress the atomic migration of Re and S precursors on the surface of the growth substrate [18]. Under such conditions the Re, S precursors could diffuse rapidly on the surfaces of the ReS_2 sheets and attach to the exposed sheets edges contributing to the vertical growth mode.

Figures 2(a) and (b) illustrate the top and side views of the crystal structure of ReS_2 with triclinic symmetry. In striking contrast to most hexagonal TMDs, ReS_2 crystallizes in a distorted 1 T structure with Re atoms forming zigzag chains along the b lattice vector direction (indicated by the red dashed line in figure 2(a)). We have carried out XRD theta/2theta scans on the ReS_2 film, as shown in figure 2(c). Peaks at 14.31°, 28.75°, and 43.78° are observed in the XRD pattern, which are in accordance with the (001), (002), (003) peaks of anorthic ReS_2. The 2theta of these peaks are slightly smaller than the bulk values, which indicates that the CVD crystal in the out of plane direction is relaxed as compared with the bulk. The presence of {001} planes in the theta/2theta XRD pattern can be explained by the bending and tilting of the ReS_2 sheets as shown in figure 1(e). The crystal structure was further studied by using aberration-corrected STEM, with the electron beam perpendicular to the flake basal plane. The high-angle annular dark-field STEM image shown in figure 2(d) matches well with the top view of the ReS_2 structure in figure 2(a), and clearly shows a 001 lattice arrangement for the few-layer ReS_2 flake. The corresponding fast Fourier transform image (figure 2(e)) displays a quasi-hexagonal pattern formed by (100), (010) reflections, which is in good accordance with previous studies [19].

The humidity sensing setup is shown in figure 5 (experiment section). The as-prepared humidity sensor (figure 1) without any modification was placed in an environmental chamber. The humidity level in the environmental chamber was controlled by adjusting the mixing ratio of dry to wet nitrogen obtained by

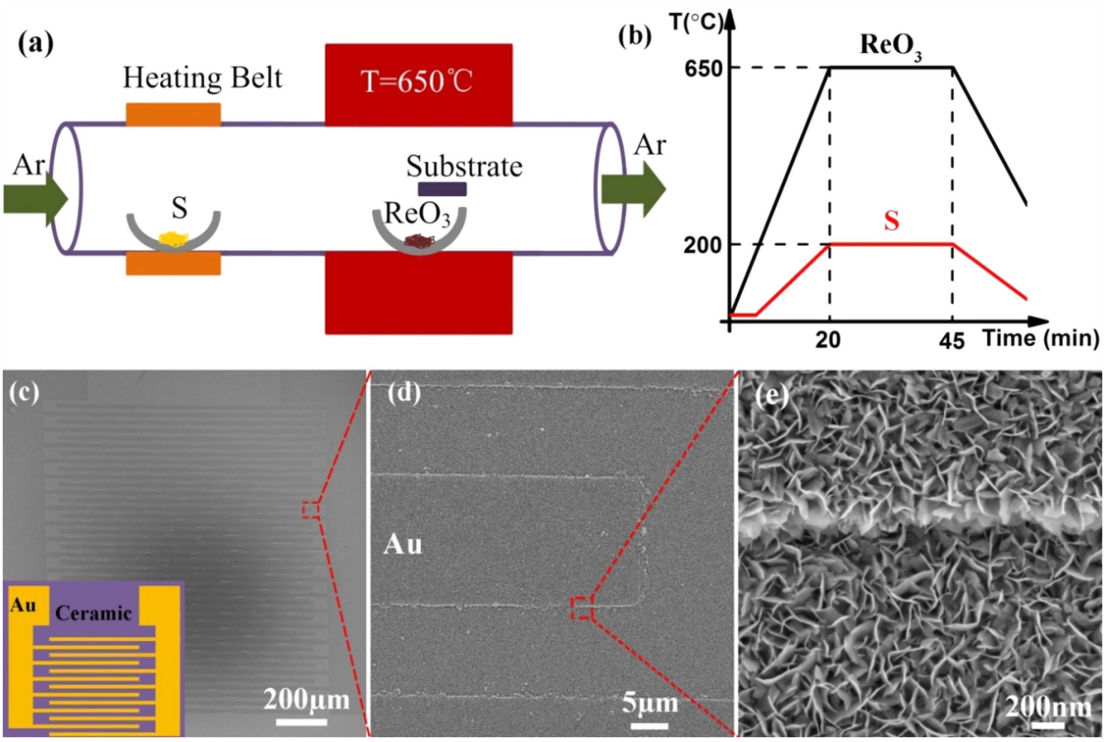

Figure 1. (a) Schematic illustration of the experimental set-up for CVD-growth of ReS_2. (b) Temperature profiles of the ReS_2 growth process. (c) Low magnification SEM image of ReS_2 on the interdigitated electrode. Inset: schematic of the interdigitated gold electrodes on ceramic substrate. (d)–(e) Higher magnification SEM images of the ReS_2 on the interdigitated electrode. In (e), the top half is on the Au electrode, while the bottom half is on the Au electrode interval (i.e. on the insulating ceramic substrate in-between the Au fingers).

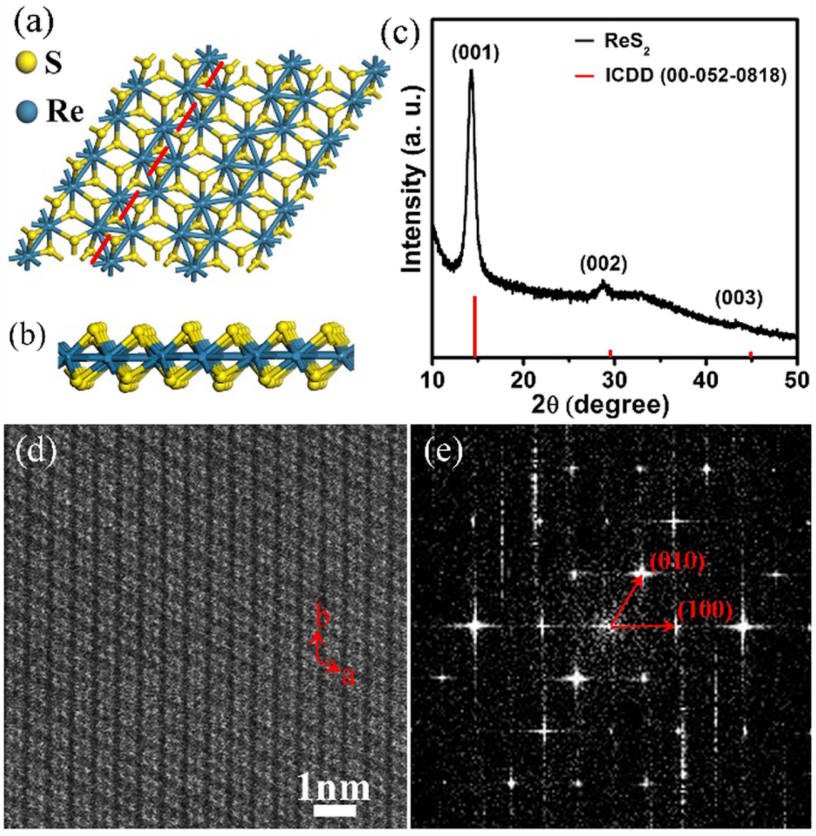

Figure 2. (a) Top view of ReS_2 crystal. (b) Side view of ReS_2 crystal. (c) XRD pattern of ReS_2 film. (d) STEM image of ReS_2 flake. (e) The corresponding fast Fourier transform (FFT) pattern of the STEM image.

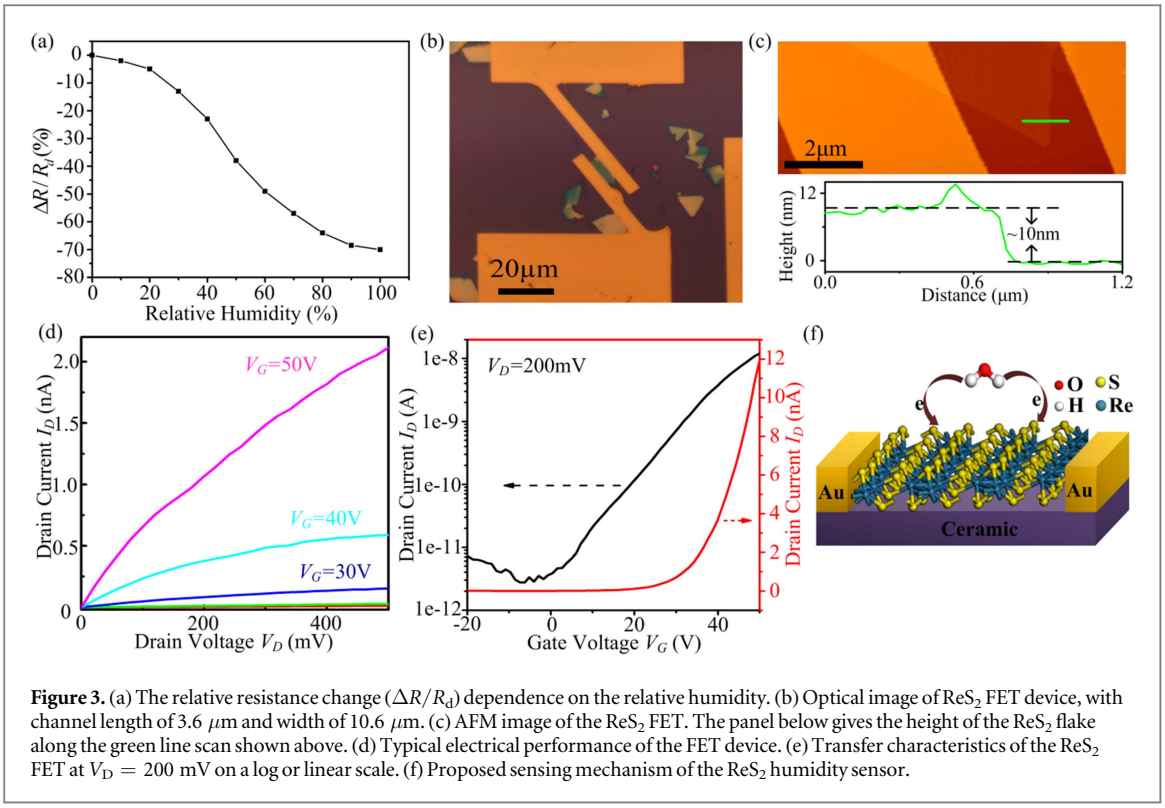

Figure 3. (a) The relative resistance change ($\Delta R/R_d$) dependence on the relative humidity. (b) Optical image of ReS_2 FET device, with channel length of 3.6 μm and width of 10.6 μm. (c) AFM image of the ReS_2 FET. The panel below gives the height of the ReS_2 flake along the green line scan shown above. (d) Typical electrical performance of the FET device. (e) Transfer characteristics of the ReS_2 FET at $V_D = 200$ mV on a log or linear scale. (f) Proposed sensing mechanism of the ReS_2 humidity sensor.

bubbling a N_2 stream through a flask with water. Details of the humidity sensing method are provided in the experimental section. Figure 3(a) illustrates the relative resistance change $\Delta R/R_d$ dependence on the relative humidity (RH), where $\Delta R = R - R_d$ and R, R_d is the resistance of the ReS_2 based sensor in humidity gas and dry nitrogen, respectively. It can be seen that the resistance decreases monotonically with increasing relative humidity. In order to investigate the underlying mechanism that is responsible for this resistance change, we extracted an individual sheet from the ReS_2 film (see experimental section for details) and constructed a back-gated FET device on a conventional SiO_2/Si substrate.

The optical image of the ReS_2 FET device is shown in figure 3(b) while the atomic force microscopy (AFM) image of the ReS_2 FET is presented in figure 3(c). The AFM line scan shows that the thickness of the ReS_2 channel is ~10 nm, which indicates that the ReS_2 flake is about 14 layers [8, 9, 15, 16]. The typical electrical performance of the FET device is presented in figure 3(d). It is found that the drain current increases with gate voltage, which indicates that the fabricated FET displays n-type semiconducting behavior consistent with previous results for CVD-grown and mechanically exfoliated ReS_2 [9, 15, 16, 19–22]. From the transfer curve shown in figure 3(e), the threshold voltage is extrapolated as ~33 V from the linear scale curve, and the on/off ratio is ~10^4 in the testing gate voltage range. The field effect carrier mobility can be calculated by using the equation: $\mu = \left[\frac{dI_D}{dV_G}\right] \times \left[\frac{L}{WC_iV_D}\right]$, where I_D is the drain current, V_G is back-gate voltage, V_D is the drain voltage of 100 mV, channel length $L = 3.6$ μm, channel width $W = 10.6$ μm and the capacitance C_i is estimated to be ~11.6 nF cm^{-2} ($C_i = \varepsilon_0\varepsilon_r/d$, where ε_0 is the dielectric constant, $\varepsilon_r = 3.9$ and $d = 300$ nm). The calculated field effect mobility of ReS_2 at $V_G = 50$ V is ~0.32 cm^2 V^{-1} s^{-1}. Since our ReS_2 film exhibits n-type behavior, the humidity sensing mechanism can be explained by n-doping of the ReS_2 sheets as shown schematically in figure 3(f). The electrical conduction of the ReS_2 film is dominated by electrons. H_2O molecules absorbed on the surfaces of the vertically oriented ReS_2 sheets will donate electrons to the n-type ReS_2, which increases the carrier concentration (electrons) in the channel between the interdigitated gold electrodes, thereby increasing the conductance. Note that this is in contrast to the carbon nanotube (CNT) based humidity sensor in Han *et al*'s work [23], where the resistance increased with relative humidity due to the reduction of hole density in the p-type CNT.

Figure 4(a) illustrates a typical single-cycle response of the ReS_2 based sensor with different relative humidity values. It is observed that the resistance of the ReS_2 sensor decreases rapidly on exposure to moisture. After the humidity gas is switched off, the resistance quickly recovers to almost 100% of the original value. The response and recovery behavior is an important metric to evaluate the performance of a humidity sensor [24]. The response and recovery time of a sensor are defined as the time taken for the resistance change to reach ~90% of the steady state value. For our moisture sensor, the response and recovery time (figure 4(a)) are ~20 s and ~10 s, respectively. As

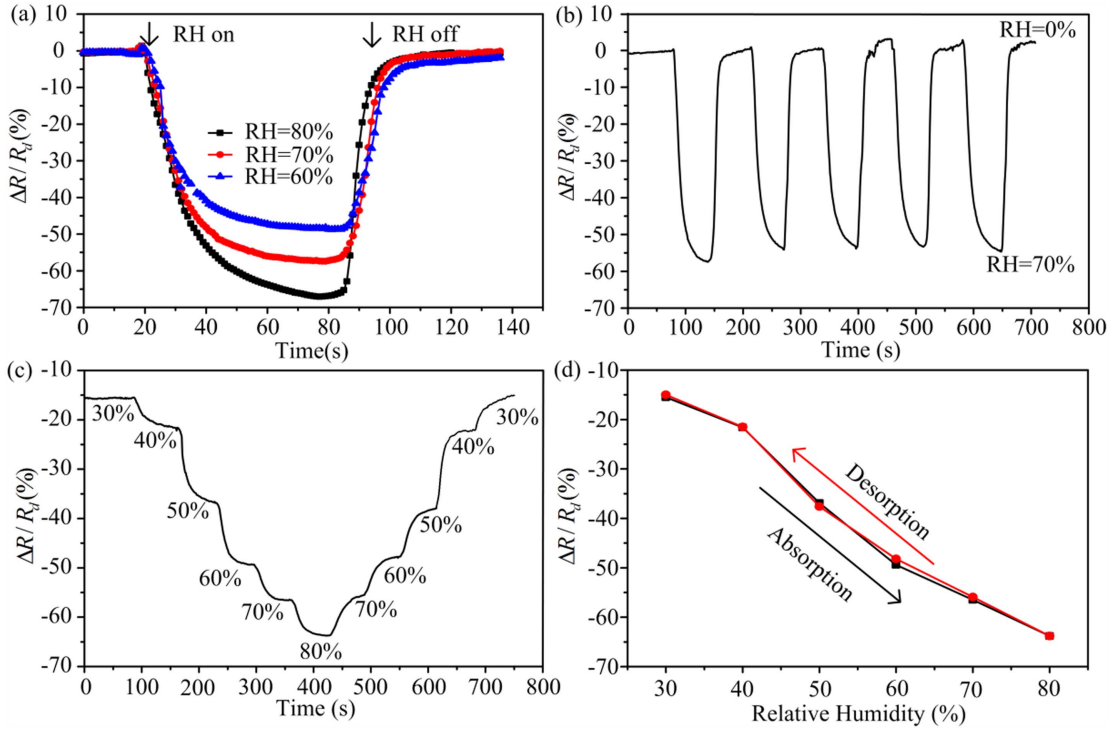

Figure 4. (a) Single-cycle response of the ReS_2 based sensor with different relative humidity values. (b) Repeated response of the ReS_2 sensor with the relative humidity changing from 0% to ~70%. (c) Step-like changes in electrical conductivity with time as the relative humidity is swept from 30% to 80% and then back to 30%. (d) Corresponding humidity hysteresis characteristics of ReS_2 humidity sensor.

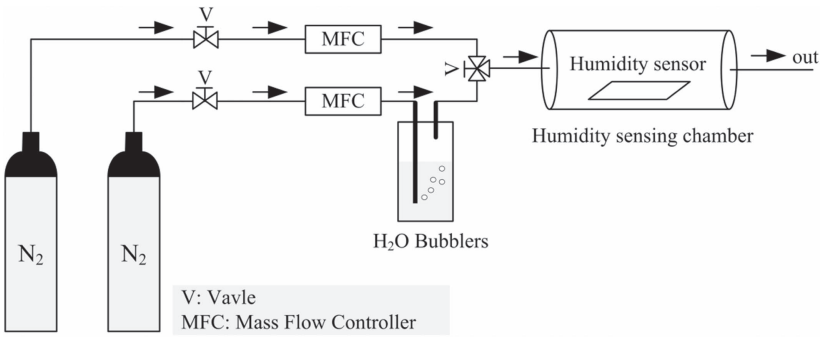

Figure 5. Schematic diagram of the humidity sensing setup.

compared to the previously reported CNT film [23], ZnO nanosheets [24] and VS_2 nanosheets [25] based humidity sensors, the ReS_2 sensor in this work exhibits faster response and recovery behavior. The faster response is presumably a result of the vertical orientation of the ReS_2 in our film, which exposes the entire surface of the nanosheets enabling rapid adsorption and desorption of water. Although some previous humidity sensors [11–14] have shown better performance for response/recovery time, our sensor is produced by a relatively simple (1-step) manufacturing process and exhibits excellent reversibility (see figures 4(c) and (d)). Figure 4(b) reveals reversible switching behavior for the ReS_2 sensor when switching on and off the humidity (RH = 70%). In every cycle, the sensor responds quickly (in ~20 s) upon exposure to humidity and recovers (in ~10 s) close to the original point after the humidity is removed. We have verified this performance for several different sensor devices indicating that the results are reproducible.

Hysteresis is a common limitation for commercial metal oxide based humidity sensors [24, 26], and results from incomplete water desorption. It is crucial to minimize the hysteresis effect for practical applications. Hysteresis can be quantified by using the relation: $|(\Delta R_{abs}/R_d - \Delta R_{des}/R_d)/(\Delta R_{abs}/R_d)| \times 100\%$, where $\Delta R_{abs}/R_d$ and $\Delta R_{des}/R_d$ are the relative resistance change in the absorption and desorption process, respectively. In

order to study the hysteresis effect of our ReS_2 sensor, the relative humidity was swept from 30% to 80% and back to 30% in steps of 10%. Figure 4(c) presents the step-like changes with time in the response as the relative humidity is varied, and figure 4(d) shows the corresponding hysteresis characteristics, showing that the ReS_2 sensor exhibits excellent reversibility (with hysteresis value <1.5%). This indicates that H_2O is rapidly desorbed from the ReS_2 and there is minimal residual water left on the ReS_2 nanosheets. Compared to TiO_2/LiCl [26] and supramolecularly modified graphene composite [13] based humidity sensors, the ReS_2 sensor device shows significantly less hysteresis effect.

Conclusion

In summary, we report a robust and high performance humidity sensor device featuring vertically oriented and densely packed ReS_2 nanosheets grown on an interdigitated electrode by CVD. The fabricated ReS_2 sensors exhibited high sensitivity, fast response and recovery times, and excellent reversibility with little hysteresis effect. The direct (1-step) growth of the ReS_2 films on an interdigitated electrode (without any transfer using wet chemistry or e-beam lithography) as in our device has important practical benefits for mass production and operation of such sensor devices in a reproducible manner.

Experimental section

Preparation of ReS_2 thin film

The substrate is an interdigitated gold electrode (width: ~20 μm, spacing: ~10 μm, NanoSPR Devices) pre-patterned on an insulating ceramic wafer. The substrate was washed thoroughly with acetone followed by methanol and iso propyl alcohol and dried with nitrogen. Then few-layer ReS_2 nanosheets were synthesized in a horizontal tube furnace equipped with a 1 inch diameter quartz tube. An alumina boat containing 200 mg of sulfur(⩾99.9% Alfa Aesar) was placed upstream in the quartz tube. The substrate was put face down above another alumina boat containing ~2 mg of ReO_3(⩾99.9% AlfaAesar) and placed in the center of the furnace. The quartz tube was pumped and flushed with nitrogen gas in order to remove air. The furnace was then ramped to ~650 °C in ~11 min and held at ~650 °C for ~25 min with a constant flow rate of argon at ~20 sccm under atmospheric pressure. After the growth cycle was completed, the system was cooled down to room temperature.

FET device fabrication and electronic performance

The ReS_2 flakes are transferred to the 300 nm SiO_2/n++Si substrates prior to device fabrication. A drop of 2-propanol was deposited over the ReS_2 flakes, and the SiO_2/Si substrate was placed directly on the ReS_2 sample, pulling it into contact with the ReS_2 flakes while naturally drying. Some ReS_2 flakes attached on the SiO_2/Si substrate after separation. The ReS_2 was patterned using Nabity Pattern Generation System e-beam lithography equipped in Carl Zeiss Supra SEM, and Ti/Au (5 nm /50 nm) electrodes were deposited by e-beam evaporation. The n++ Si was used as the back gate. The typical *I–V* characteristics were measured by a HP4155B semiconductor parameter analyzer.

Characterization method

SEM images were taken using Carl Zeiss Supra SEM, and the AFM images were taken by PSI XE100 AFM in contact mode. The AFM tip (μmash, HQ: CSC17/AL BS) used has a tip radius of 8 nm, a force constant of 0.18 N m^{-1}, and a resonant frequency of 13 kHz. Aberration-corrected STEM imaging experiments were performed with a Nion UltraSTEM-100, equipped with a cold field emission electron source and a corrector of 3rd and 5th order aberrations [27]. The microscope was operated at 100 kV accelerating voltage and the convergence semi-angle of the incident probe was set to ~30 mrad. The high-angle annular dark field images—also known as Z-contrast—were collected from ~86 to 200 mrad half-angle range.

Humidity sensing method

The humidity sensing setup is shown in figure 5. The as-prepared humidity sensor (figure 1) was placed in an environmental chamber for the tests. The wet gas flow was obtained by bubbling a N_2 stream through a flask with water. The humidity level in the environmental chamber was controlled by adjusting the mixing ratio of dry to wet nitrogen using a mixing system equipped with mass flow controllers. The total flow was set to ~500 sccm in our experiments. The resistance of sensor was measured by an Agilent 34401A instrument with four-probe method. The four-probe method eliminates the effect of contact resistances. All tests were conducted at room temperature and atmospheric pressure.

Acknowledgments

NK and TML acknowledge funding support from the USA National Science Foundation (Award Numbers 1234641, 1435783, 1510828, and 1608171). Microscopy research was conducted as part of a user proposal through ORNL's Center for Nanophase Materials Sciences, which is a US Department of Energy, Office of Science User Facility (JCI). AY and MR acknowledge support from the National Key Basic Research Program of China (973Program) (2015CB251002), National Science Foundation of China (Grant No.51521065 and51221005), China Postdoctoral Science Foundation (2015M572558) and the State Key Laboratory of Electrical Insulation and Power Equipment (No. EIPE16307).

References

[1] Allen M J, Tung V C and Kaner R B 2009 Honeycomb carbon: a review of graphene *Chem. Rev.* **110** 132–45

[2] Wang Q H, Kalantar-Zadeh K, Kis A, Coleman J N and Strano M S 2012 Electronics and optoelectronics of two-dimensional transition metal dichalcogenides *Nat. Nanotechnol.* **7** 699–712

[3] Yavari F, Castillo E, Gullapalli H, Ajayan P M and Koratkar N 2012 High sensitivity detection of NO_2 and NH_3 in air using chemical vapor deposition grown graphene *Appl. Phys. Lett.* **100** 203120

[4] Yi J, Lee J M and Park W I 2011 Vertically aligned ZnO nanorods and graphene hybrid architectures for high-sensitive flexible gas sensors *Sensors Actuators* B **155** 264–9

[5] Schedin F, Geim A K, Morozov S V, Hill E W, Blake P, Katsnelson M I and Novoselov K S 2007 Detection of individual gas molecules adsorbed on graphene *Nat. Mater.* **6** 652–5

[6] Yavari F and Koratkar N 2012 Graphene-based chemical sensors *J. Chem. Phys. Lett.* **3** 1746–53

[7] Perkins F K, Friedman A L, Cobas E, Campbell P M, Jernigan G G and Jonker B T 2013 Chemical vapor sensing with monolayer MoS_2 *Nano Lett.* **13** 668–73

[8] Tongay S, Sahin H, Ko C, Luce A, Fan W, Liu K, Zhou J, Huang Y-S, Ho C-H and Yan J 2014 Monolayer behaviour in bulk ReS_2 due to electronic and vibrational decoupling *Nat. Commun.* **5** 3252

[9] Yang S, Kang J, Yue Q, Coey J M D and Jiang C 2016 Defect-modulated transistors and gas-enhanced photodetectors on ReS_2 nanosheets *Adv. Mater. Interfaces* **3** 1500707

[10] Chen Z and Lu C 2005 Humidity sensors: a review of materials and mechanisms *Sens. Lett.* **3** 274–95

[11] Wu T-F and Hong J-D 2016 Synthesis of water-soluble dopamine–melanin for ultrasensitive and ultrafast humidity sensor *Sensors Actuators* B **224** 178–84

[12] Borini S, White R, Wei D, Astley M, Haque S, Spigone E, Harris N, Kivioja J and Ryhanen T 2013 Ultrafast graphene oxide humidity sensors *ACS Nano* **7** 11166–73

[13] Wang S, Chen Z, Umar A, Wang Y, Tian T, Shang Y, Fan Y, Qi Q and Xu D 2015 Supramolecularly modified graphene for ultrafast responsive and highly stable humidity sensor *J. Phys. Chem.* C **119** 28640–7

[14] Chi H, Liu Y J, Wang F and He C 2015 Highly sensitive and fast response colorimetric humidity sensors based on graphene oxides film *ACS Appl. Mater. Interfaces* **7** 19882–6

[15] Keyshar K *et al* 2015 Chemical vapor deposition of monolayer rhenium disulfide (ReS_2) *Adv. Mater.* **27** 4640–8

[16] He X, Liu F, Hu P, Fu W, Wang X, Zeng Q, Zhao W and Liu Z 2015 Chemical vapor deposition of high-quality and atomically layered ReS_2 *Small* **11** 5423–9

[17] Zhang E, Jin Y, Yuan X, Wang W, Zhang C, Tang L, Liu S, Zhou P, Hu W and Xiu F 2015 ReS_2-based field-effect transistors and photodetectors *Adv. Funct. Mater.* **25** 4076–82

[18] Gao J, Li L, Tan J, Sun H, Li B, Idrobo J C, Singh C V, Lu T-M and Koratkar N 2016 Vertically oriented arrays of ReS_2 nanosheets for electrochemical energy storage and electrocatalysis *Nano Lett.* **16** 3780–7

[19] Liu E *et al* 2015 Integrated digital inverters based on two-dimensional anisotropic ReS_2 field-effect transistors *Nat. Commun.* **6** 6991

[20] Xu K, Deng H-X, Wang Z, Huang Y, Wang F, Li S-S, Luo J-W and He J 2015 Sulfur vacancy activated field effect transistors based on ReS_2 nanosheets *Nanoscale* **7** 15757–62

[21] Corbet C M, McClellan C, Rai A, Sonde S S, Tutuc E and Banerjee S K 2014 Field effect transistors with current saturation and voltage gain in ultrathin ReS_2 *ACS Nano* **9** 363–70

[22] Lin Y-C, Komsa H-P, Yeh C-H, Björkman T R, Liang Z-Y, Ho C-H, Huang Y-S, Chiu P-W, Krasheninnikov A V and Suenaga K 2015 Single-layer ReS_2: two-dimensional semiconductor with tunable in-plane anisotropy *ACS Nano* **9** 11249–57

[23] Han J-W, Kim B, Li J and Meyyappan M 2012 Carbon nanotube based humidity sensor on cellulose paper *J. Phys. Chem.* C **116** 22094–7

[24] Tsai F-S and Wang S-J 2014 Enhanced sensing performance of relative humidity sensors using laterally grown ZnO nanosheets *Sensors Actuators* B **193** 280–7

[25] Feng J, Peng L, Wu C, Sun X, Hu S, Lin C, Dai J, Yang J and Xie Y 2012 Giant moisture responsiveness of VS2Ultrathin nanosheets for novel touchless positioning interface *Adv. Mater.* **24** 1969–74

[26] Buvailo A I, Xing Y, Hines J, Dollahon N and Borguet E 2011 TiO_2/LiCl-based nanostructured thin film for humidity sensor applications *ACS Appl. Mater. Interfaces* **3** 528–33

[27] Krivanek O L, Corbin G J, Dellby N, Elston B F, Keyse R J, Murfitt M F, Own C S, Szilagyi Z S and Woodruff J W 2008 An electron microscope for the aberration-corrected era *Ultramicroscopy* **108** 179–95